CHEMISTRY
A EUROPEAN JOURNAL

DOI: 10.1002/chem.200600261

A Facile Route to the Non-IPR Fullerene $Sc_3N@C_{68}$: Synthesis, Spectroscopic Characterization, and Density Functional Theory Computations (IPR = Isolated Pentagon Rule)

Shangfeng Yang,[a] Martin Kalbac,[a, c] Alexey Popov,[b] and Lothar Dunsch*[a]

Abstract: Owing to the unique feature of the non-IPR D_3 (isomer 6140) C_{68} cage (IPR = isolated pentagon rule), $Sc_3N@C_{68}$ has been attracting great interest in the fullerene community. Herein we report the first high-yield synthesis of $Sc_3N@C_{68}$ by the "reactive gas atmosphere" method and its facile isolation by single-step HPLC to a high purity ($\geq 99\,\%$). Thus, $Sc_3N@C_{68}$ is isolated in sufficient quantities for its further spectroscopic characterization, while the high purity of the sample ensures the reliability of the spectroscopic data obtained. In particular, the electronic and vibrational structures of $Sc_3N@C_{68}$ were studied in detail experimentally and by theoretical computations. The assignment of the observed absorption bands to particular electronic transitions is given in detail on the basis of time-dependent DFT computations. Vibrational spectroscopy of $Sc_3N@C_{68}$ reveals good agreement between the measured spectra and the theoretically calculated spectra. A detailed assignment of the vibrational modes, including the Sc_3N cluster modes, cage modes, and vibrations of the adjacent pentagons are discussed. This study reveals that the effect of Sc_3N encapsulation in the cage is much more complicated than just a formal transfer of six electrons. Consequently the electronic and vibrational spectra of the carbon cage in $Sc_3N@C_{68}$ cannot be adequately understood on the basis of a C_{68}^{6-} cage alone.

Keywords: density functional calculations · fullerenes · host–guest systems · structure elucidation · vibrational spectroscopy

Introduction

As a new class of fullerenes hosting a trimetallic nitride cluster, trimetallic nitride endohedral fullerenes (clusterfullerenes) have been attracting a great deal of interest because it is possible to tune the trapped metal atoms and to stabilize a large variety of cage sizes, including different isomeric structures.[1–7] Soon after the discovery of $Sc_3N@C_{80}$,[3] a non-IPR clusterfullerene $Sc_3N@C_{68}$ as well as $A_xSc_{3-x}N@C_{68}$ (x = 0–2; A = Tm, Er, Gd, Ho, La; IPR = isolated pentagon rule) were isolated in the year 2000, after the first non-IPR metallofullerene $Sc_2@C_{66}$ had been reported.[8,9] The unique feature of $Sc_3N@C_{68}$ is the Sc_3N cluster that is encapsulated in a D_3 (isomer 6140), non-IPR C_{68} cage, as determined by X-ray crystallography and NMR spectroscopy,[9,10] which makes this fullerene particularly interesting. However, only limited spectroscopic data on $Sc_3N@C_{68}$ has been reported to date,[9] chiefly owing to its lower accessibility compared with that of other clusterfullerenes, such as $Sc_3N@C_{78}$ and $Sc_3N@C_{80}$, which have IPR-obeyed cages.[6,7] Therefore, a detailed discussion on the synthesis of this fullerene with respect to enhancement of the yield is needed. Furthermore, a very recent study focused on theoretical calculations of the molecular structure of $Sc_3N@C_{68}$ on the basis of the ^{13}C NMR spectrum.[11–13] A deeper understanding of this peculiar molecule, including the electronic and vibrational structures, appears to be quite intriguing. No detailed experimental or theoretical studies of these structures have been carried out to date.

Although the isomeric structure of the cage has been well established,[1–7] the structure and stability of the cluster and

[a] Dr. S. Yang, Dr. M. Kalbac, Prof. Dr. L. Dunsch
Group of Electrochemistry and Conducting Polymers
Leibniz-Institute for Solid State and Materials Research
Dresden, 01171 Dresden (Germany)
Fax: (+49) 351-4659-811
E-mail: l.dunsch@ifw-dresden.de

[b] Dr. A. Popov
Department of Chemistry, Moscow State University
Leninskiye Gory, 119992 Moscow (Russia)

[c] Dr. M. Kalbac
J. Heyrovský Institute of Physical Chemistry
Academy of Sciences of the Czech Republic
Dolejškova 3, 18223 Prague 8 (Czech Republic)

Supporting information for this article is available on the WWW under http://www.chemeurj.org/ or from the author.

Pagination corrected Oct. 17, 2006

its charge transfer to the cage are rarely studied because such information could not be provided directly by X-ray crystallography and NMR spectroscopy. As we have previously demonstrated, vibrational spectroscopy is a powerful tool for the structural analysis of fullerenes owing to its high structural sensitivity on the one hand and because of its higher time resolution relative to NMR spectroscopy on the other.[1,2,5–7] Specifically, for clusterfullerenes, the structure of the encaged cluster can be probed by its vibrational patterns in IR and Raman spectra.

We report herein on the high-yield synthesis of $Sc_3N@C_{68}$ by the "reactive gas atmosphere" method and the first experimental vibrational and electronic absorption spectroscopic studies. Both the electronic and vibrational structures of $Sc_3N@C_{68}$ have been further studied by means of theoretical computations. The assignment of the observed absorption bands to the electronic transitions is given in detail. The measured IR and Raman spectra are compared with those computed by using DFT in order to assign the specific vibrational modes.

Results and Discussion

Synthesis of the $Sc_3N@C_{68}$ clusterfullerene: The $Sc_3N@C_{68}$ clusterfullerene can be obtained in a high yield by using the "reactive gas atmosphere" method.[1,2,4–7] A typical chromatogram of an extracted mixture of $Sc_3N@C_{2n}$ fullerenes is shown in Figure 1 (curve a), which, in combination with mass spectroscopic (MS) analysis, indicates the formation of $Sc_3N@C_{2n}$ clusterfullerenes as the main products. According to the integrated peak area, it is clear that the yield of $Sc_3N@C_{68}$ ($t_R = 19.3$ min, m/z: 965) exceeds those of the empty fullerenes C_{60} and C_{70} and is at least three orders of magnitude higher than that of C_{84} by assuming that the absorption coefficient of $Sc_3N@C_{68}$ at the detection wavelength of 320 nm is comparable to those of the empty fullerenes. Such a high yield has never been achieved by using the "trimetallic nitride template" (TNT) method previously reported.[3,9] In general, C_{84} could be regarded as the reference for estimating the relative yields of the conventional endohedral metallofullerenes.[6b,14,15] Based on this reference, it could be inferred that the yield of $Sc_3N@C_{68}$ is also several orders of magnitude higher than that of all the endohedral metallofullerenes. On the other hand, among the $Sc_3N@C_{2n}$ clusterfullerenes, only three $Sc_3N@C_{2n}$ ($2n = 78$, 80) clusterfullerenes (A–C in Figure 1a, $t_R \approx 31.0$–38.0 min) exceed $Sc_3N@C_{68}$ in yield, while the yields of clusterfullerenes with cages larger than C_{80} and consequently larger retention times, are significantly lower than that of $Sc_3N@C_{68}$. An interpretation of the strongly enhanced yields of the clusterfullerenes by using the facile "reactive gas atmosphere" method has already been proposed.[6a]

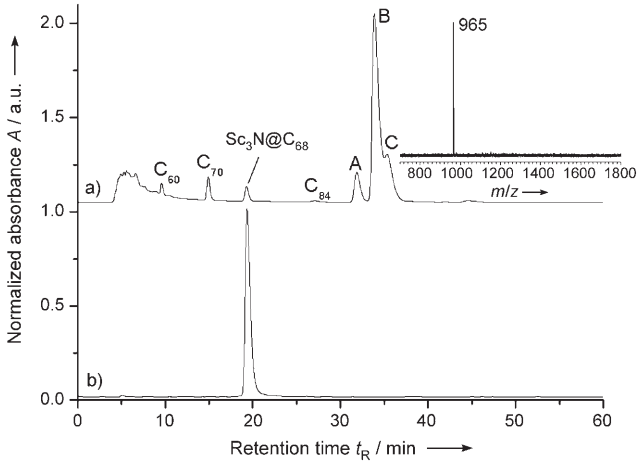

Figure 1. Chromatograms of a) a $Sc_3N@C_{2n}$ fullerene extract mixture synthesized by using the "reactive gas atmosphere" method and b) $Sc_3N@C_{68}$ (isolated with linear combination of two 4.6×250 mm Buckyprep columns; flow rate 1.6 mL min^{-1}; injection volume 100 μL; toluene as eluent (mobile phase); 40 °C). A: $Sc_3N@C_{78}$; B: $Sc_3N@C_{80}$(I); C: $Sc_3N@C_{80}$(II). Inset: positive-ion LD-TOF mass spectrum of the isolated $Sc_3N@C_{68}$.

Owing to such a high-yield production, $Sc_3N@C_{68}$ is readily isolated by single-step HPLC to a high purity (≥99%), which is ascertained by further HPLC analysis (curve b in Figure 1) and laser desorption time-of-flight (LD-TOF) MS analysis (inset of Figure 1). Such a high purity ensures the reliability of the following spectroscopic characterization.

Electronic structure of $Sc_3N@C_{68}$: The UV/Vis/NIR spectrum of the isolated $Sc_3N@C_{68}$ dissolved in toluene (Figure 2a) exhibits the characteristic electronic absorptions that are chiefly attributable to π–π* transitions of fullerene cages and is very rich in features. The measured UV/Vis/NIR spectrum of $Sc_3N@C_{68}$ completely agrees with the spectrum measured in CS_2 reported in ref. [9]. Therefore, the same isomeric structure of the cage (D_3) could be unambiguously assigned to our sample because it is known that the electronic spectrum of a fullerene is strongly dependent on its isomeric structure.[6,7,14,15] However, the detailed analysis of the UV/Vis/NIR spectrum of $Sc_3N@C_{68}$ is not given in ref. [9] and other literature despite its importance. Based on the absorption spectral onset at $\lambda \approx 1200$ nm, the optical band gap of $Sc_3N@C_{68}$ is estimated to be 1.1 eV,[1–9,14,15] indicating that $Sc_3N@C_{68}$ has a large band gap and is hence a stable fullerene. The optical band gap of $Sc_3N@C_{68}$ is significantly smaller than those of $Sc_3N@C_{78}$ and $Sc_3N@C_{80}$(I, II),[7a,b] suggesting the strong influence of the non-IPR cage on its electronic structure. The strongest absorption of $Sc_3N@C_{68}$ has maxima at $\lambda = 560$ and 600 nm, and there are several shoulder peaks at 627, 659, and 673 nm. This pattern is significantly stronger than the HOMO–LUMO transition, which has a doublet structure with absorption maxima at $\lambda = 785$ and 824 nm (see inset of Figure 2a).

The electronic structure of $Sc_3N@C_{68}$ was also studied by means of time-dependent (TD) DFT computations. Figure 2b compares the experimental absorption spectrum of $Sc_3N@C_{68}$ (curve A) to the calculated spectrum, including excitation energies and oscillator strengths (f) of $Sc_3N@C_{68}$ (curve B). Taking into account the systematic underestima-

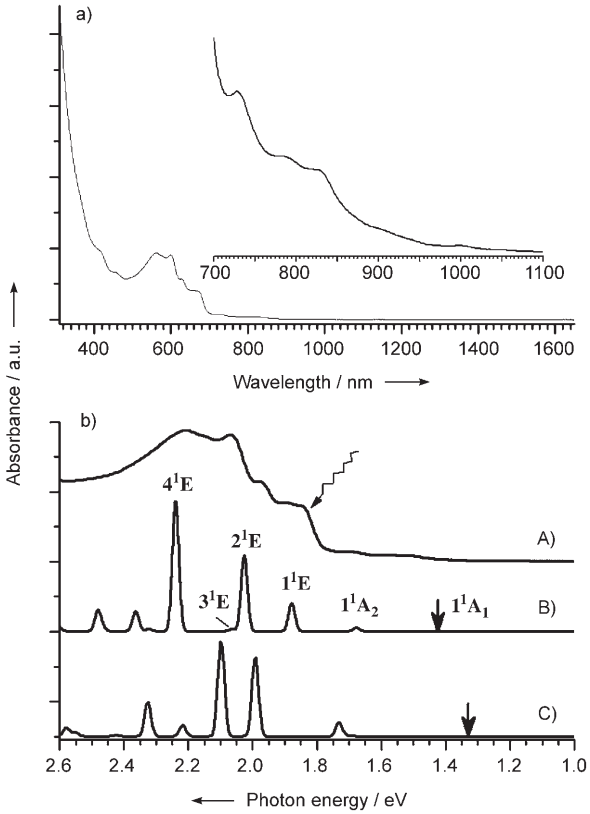

Figure 2. a) UV/Vis/NIR spectrum of $Sc_3N@C_{68}$ dissolved in toluene. The inset shows the enlarged spectral range (700–1100 nm). b) Experimental UV/Vis/NIR spectrum of $Sc_3N@C_{68}$ (A, converted from a) compared to the calculated spectra of $Sc_3N@C_{68}$ (B), and C_{68}^{6-} (C) (up-shifted by 0.1 eV for the sake of comparison) by TD-DFT simulations. The wavy arrow denotes the wavelength of the excitation laser line. The arrows in curves B and C represent the dipole-forbidden HOMO→LUMO transitions.

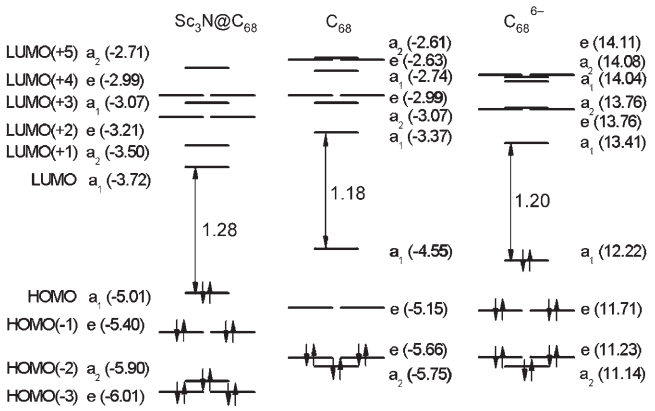

Figure 3. MO levels in $Sc_3N@C_{68}$, C_{68}, and C_{68}^{6-}. The electrons in C_{68}^{6-} are formally unbound, and for the sake of comparison, the energy levels in C_{68}^{6-} were shifted by 16.89 eV to equalize the energies of the occupied a_2 MOs.

In the higher energy region (1.8–2.5 eV), the experimental spectrum exhibits very rich structures specifically with the strongest absorption as discussed above. However, TD-DFT computations predict only three intense transitions in this energy region, indicating that some of the observed features may be attributable to vibronic bands. Therefore, we attribute the absorption band at 1.842 eV to the $S_0 \rightarrow 1^1E$ transition with leading HOMO(−1)→LUMO and HOMO→LUMO(+2) excitations. As such, the absorption at 2.066 eV is assigned to the HOMO→LUMO(+2) transition ($S_0 \rightarrow 2^1E$), while the broad intense band at 2.214 eV is assigned to the HOMO→LUMO(+4) transition ($S_0 \rightarrow 4^1E$). The proposed correlation of the observed absorption bands with the assigned transitions is summarized in Table 1.

Table 1. Low-energy excitations in $Sc_3N@C_{68}$: experimental (exptl) data and TD-DFT calculations (calcd).

S_n	E [eV] exptl (λ [nm])	calcd	f	Leading configurations
S_1–1^1A_1	1.505 (824), 1.579 (785)	1.326		HOMO→LUMO
S_2–1^1A_2	1.701 (728)	1.565	0.0013	HOMO→LUMO(+1)
S_3–1^1E	1.842 (673), 1.881 (659), 1.977 (627)	1.768	0.0099	HOMO(−1)→LUMO, HOMO→LUMO(+2)
S_4–2^1E	2.066 (600)	1.917	0.0274	HOMO→LUMO(+2)
S_5–3^1E		1.950	0.0008	HOMO(−1)→LUMO(+1)
S_6–2^1A_1		2.004		HOMO→LUMO(+3)
S_7–4^1E	2.214 (560)	2.128	0.0450	HOMO→LUMO(+4)

tion of excitation energies by TD-DFT,[16] the latter provides a reasonable agreement with the experimental data and hence enables us to provide a tentative interpretation of the electronic structure of $Sc_3N@C_{68}$. The MO levels in $Sc_3N@C_{68}$, obtained by means of DFT computations, are shown in Figure 3 in comparison with those in C_{68} and C_{68}^{6-}. As both the HOMO and LUMO in $Sc_3N@C_{68}$ have A_1 symmetries, the HOMO→LUMO transition is dipole-forbidden. The predicted energy of this transition is 1.326 eV, and we propose that the very weak experimental features at 1.505 eV (824 nm) and 1.579 eV (785 nm) (see inset of Figure 2a) result from vibronic activation of HOMO→LUMO excitation. The first dipole-allowed transition is HOMO→LUMO(+1), because LUMO(+1) has A_2 symmetry, and in the experimental spectrum it appears as a weak band at 1.701 eV (728 nm).

Furthermore, the calculated electronic spectrum of C_{68}^{6-} (Figure 2b, curve C) appears to be dramatically different from that of $Sc_3N@C_{68}$. This is a clear manifestation of the difference in their electronic structures, which can be also established by a comparison of the relative MO levels in these species (Figure 3). Therefore, it is worth noting that, because the cage MOs in $Sc_3N@C_{68}$ are hybridized with those of the Sc_3N cluster, the electronic structure of $Sc_3N@C_{68}$ is substantially different from the one that could simply result from a formal six-electron transfer from the Sc_3N cluster to the empty C_{68} cage.[9,13]

Vibrational spectra of $Sc_3N@C_{68}$: The vibrational structure of $Sc_3N@C_{68}$ was studied both experimentally and theoretically. Figure 4 compares the measured FTIR spectrum of

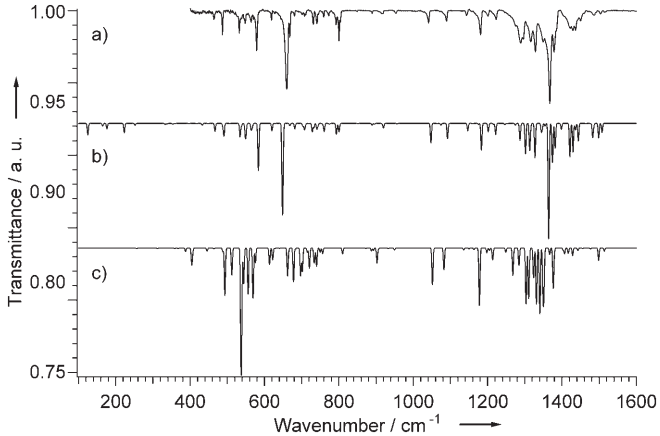

Figure 4. FTIR spectrum of $Sc_3N@C_{68}$ (a) compared with the calculated IR spectra of $Sc_3N@C_{68}$ (b) and C_{68}^{6-} (c). The calculated spectra were shifted by 10 cm^{-1} to higher wavenumbers for a better comparison.

$Sc_3N@C_{68}$ (curve a) to the calculated spectra of $Sc_3N@C_{68}$ (curve b) and C_{68}^{6-} (curve c). The measured FTIR spectrum of $Sc_3N@C_{68}$ (curve a) is dramatically different from those of $Sc_3N@C_{78}$ and $Sc_3N@C_{80}$(I, II) and exhibits a relatively large number of lines owing to its reduced cage symmetry compared with the latter ones.[7a,b] We used the same method as previously reported by our group[6b,7a,b,17] to assign the most intense low-energy IR line at about 660 cm^{-1} to the antisymmetric Sc–N stretching vibration, while the remaining lines are mainly contributions from the tangential and radial cage modes.[6b,7a,b,17] Regardless of the $\approx$10 cm^{-1} systematic underestimation of the vibrational frequencies, the DFT-calculated results of $Sc_3N@C_{68}$ (curve b) perfectly fit the measured IR spectrum (curve a) in terms of both the Sc–N antisymmetric stretching vibrational mode and the cage modes, thus facilitating a reasonable assignment of the vibrational bands as discussed in detail below. On the other hand, the dramatic difference between the IR spectra of $Sc_3N@C_{68}$ and C_{68}^{6-} reveals the strong influence of the encapsulated Sc_3N cluster, and consequently its charge transfer to the cage, on the vibrational structure of the clusterfullerene.

Figure 5 presents the measured Raman spectrum of $Sc_3N@C_{68}$ (curve a). The spectrum is dramatically different from that of $Sc_3N@C_{80}$(I) with the main discrepancy observed in the range of Raman shift between 500 and 850 cm^{-1}.[17] As a matter of fact, the Raman lines of $Sc_3N@C_{68}$ between 500 and 850 cm^{-1} exhibit the strongest intensities. In contrast, the intensities of the Raman lines in this range for $Sc_3N@C_{80}$(I) are dramatically lower than those from 500 cm^{-1} downwards.[17] Assuming that the vibrational modes in the range of 500–850 cm^{-1} are usually correlated with the radial modes of the carbon cages,[17] this result suggests a strong contribution of the non-IPR feature

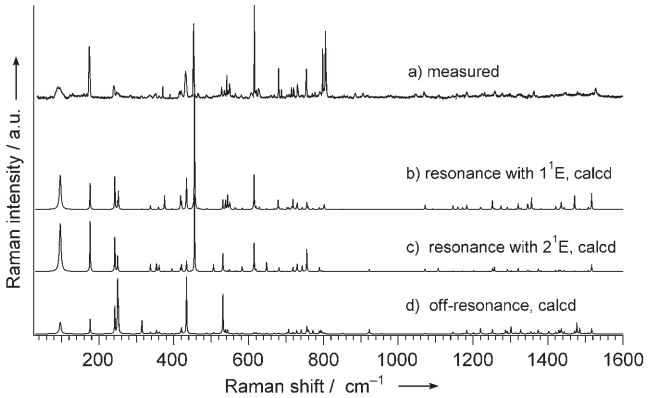

Figure 5. Raman spectrum of $Sc_3N@C_{68}$ (a) in comparison with the calculated spectra for resonance (b, c) and off-resonance (d) conditions. The calculated spectra are broadened with Lorentzian peaks with half-width at half-maximum (HWHM) 1.5 cm^{-1}, except for the 86 cm^{-1} mode that is broadened with a HWHF of 5 cm^{-1}. The calculated spectra were shifted by 10 cm^{-1} to higher wavenumbers for a better comparison.

of the C_{68} cage to the radial modes of the carbon cages, as discussed below.

The measured Raman spectrum was also compared to those spectra simulated for the resonance scattering enhanced by $S_0 \rightarrow 1^1E$ (curve b) or $S_0 \rightarrow 2^1E$ (curve c) electronic transitions, and for the off-resonance scattering condition (curve d). The latter shows a poor agreement with the experimental results because the lines that are predicted by simulation to be the most intense have a very low intensity in the measured spectrum. In fact, theory predicts that the $S_0 \rightarrow 1^1E$ dipole-allowed electron transition is quite close to the Raman excitation wavelength, thus the excitation of the spectrum with 676 nm (1.83 eV) may result in pre-resonance scattering owing to its interaction with the electron transitions observed in the absorption spectrum of $Sc_3N@C_{68}$ (Figure 2b). Indeed, the simulated spectrum with resonance is in much better agreement with the measured data and may serve as a further guide for assignment of the vibrational bands. However, it should be noted that all computed spectra severely underestimate the intensities of strong Raman lines in the 600–800 cm^{-1} range, while the intensity of the A_1 mode at 453 cm^{-1} is significantly overestimated.

The measured IR and Raman spectra of $Sc_3N@C_{68}$ are shown in Figure 6 for an overall view and its molecular structure is schematically shown in Figure 7. D_3-$Sc_3N@C_{68}$ exhibits 140 vibrational modes that are IR- or Raman-active, as shown by the irreducible representations shown in Equation (1):

$$\Gamma_{vib}(D_3\text{-}Sc_3N@C_{68}) = 35\,A_1\,(R) + 35\,A_2\,(IR) + 70\,E\,(R, IR) \quad (1)$$

in which R and IR denote Raman and IR activity, respectively. Accordingly, 105 lines are expected both in Raman and IR spectra. In this sense, the observed number of lines

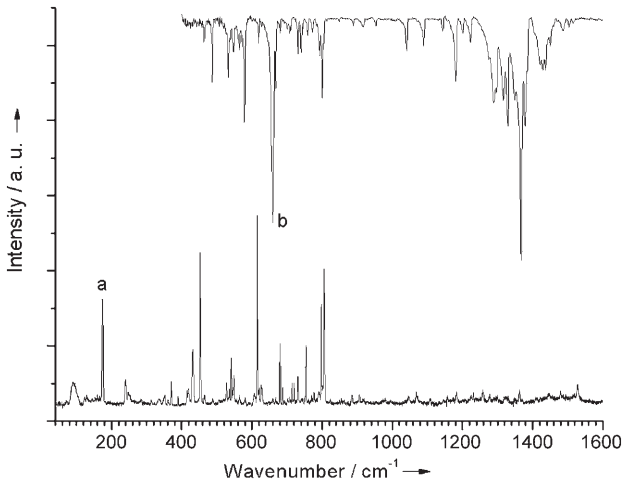

Figure 6. Experimental FTIR (top trace) and Raman spectra (lower trace) of $Sc_3N@C_{68}$ (copied from Figures 4 and 5) for comparison. The labels a and b are explained in the text.

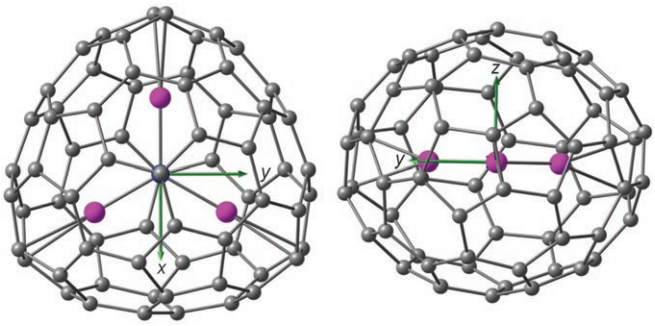

Figure 7. Schematic structure of $Sc_3N@C_{68}$ in two views. Left: along the C_3 (z) axis; right: along the C_2 (x) axis).

is much lower than that expected by the selection rule of D_3-$Sc_3N@C_{68}$ in both spectra owing to the existence of many lines with a very low intensity. Only a few lines with a relatively low intensity appear to be both IR- and Raman-active. Below we focus the detailed discussion on the assignment of some specific vibrational modes of $Sc_3N@C_{68}$ and the complete assignment of the experimental lines. A complete list of computed vibrational frequencies of $Sc_3N@C_{68}$ is given in Table S2 of the Supporting Information.

Sc_3N cluster vibrational modes: The irreducible representation for the Sc_3N cluster (including external degrees of freedom) in the D_3 symmetry group is A_1+3A_2+4E. According to DFT computations, the five lowest frequency vibrations of $Sc_3N@C_{68}$ are solely cluster modes: the two-fold degenerated vibrational E mode (rotation around the x and the y axis, Figure 7) appears as a broad Raman band at 90 cm^{-1}. The strong Raman line at 174 cm^{-1} (line a in Figure 6) corresponds to the in-plane Sc-N-Sc bending mode (E mode, calcd at 166 cm^{-1}). Three other low-frequency modes have A_2 symmetry and are therefore silent in the Raman spectrum. Another mode with a predominant cluster contribution appears as a strong IR band at 661 cm^{-1} (line b in Figure 6). This E-symmetry mode is also known as an antisymmetric Sc–N stretching vibration, which corresponds to the nitrogen atom motion in the plane of the cluster.[6b,7,16] In $Sc_3N@C_{78}$ and $Sc_3N@C_{80}$(I), the corresponding vibrations occur at 623 and 600 cm^{-1}.[7a,b] The softening of this mode with enlargement of the carbon cage is in good agreement with the elongation of Sc–N bonds in these molecules predicted by the calculations: 1.993 Å in $Sc_3N@C_{68}$, 2.012 Å in $Sc_3N@C_{78}$, and 2.034 Å in $Sc_3N@C_{80}$(I). Two remaining modes of the Sc_3N cluster are strongly coupled to the carbon cage vibrations. The highest contributions of the E translation mode ($T_{x,y}$) are calculated to be at 242 (45%) and 344 cm^{-1} (20%). In the measured Raman spectrum, only the former is observed as a weak line at 249 cm^{-1}. A totally symmetric Sc–N stretching vibration is scattered among several cage modes, with the highest contributions found at 351 (18%), 424 (26%), and 521 cm^{-1} (38%). In the measured Raman spectrum, these modes are observed at 361 (vw), 431 (m), and 528 cm^{-1} (w), respectively. The mode at 528 cm^{-1} is also characterized by the considerable contribution of Sc–C stretching vibrations as the amplitudes of the outward Sc atom motions are much higher than those of C atoms, which inevitably causes variation of the Sc–C bond lengths during the vibration. The observed vibrational modes of the Sc_3N cluster in both IR and Raman spectra and their assignments are summarized in Table 2.

Carbon cage modes: The stability of the C_{68} cage in $Sc_3N@C_{68}$ is established by a formal charge transfer of six electrons from the encaged cluster to the cage.[13] Assuming the molecular and electronic structures of the carbon cages in $Sc_3N@C_{68}$ and C_{68}^{6-} are similar, it is reasonable to propose that vibrations of these cages are also similar. Exact correlations can be obtained through projection of the $Sc_3N@C_{68}$ vibrational eigenvectors onto the space of the C_{68}^{6-} normal modes. When the vibrational displacement pattern of a $Sc_3N@C_{68}$ mode is similar to the given C_{68} mode, the contribution of the latter is close to 100%. Conversely, if a $Sc_3N@C_{68}$ mode is not similar to any C_{68}^{6-} vibration, it appears in the projection analysis as a "mixing" of different C_{68}^{6-} modes. Indeed, for more than half of the $Sc_3N@C_{68}$ vibrations, the projection analysis revealed strong similarities with C_{68}^{6-} modes, but at the same time, comparison of the calculated IR spectra shows that intensity patterns for $Sc_3N@C_{68}$ and C_{68}^{6-} are substantially different (Figure 4). For instance, the corresponding vibrations of $Sc_3N@C_{68}$ usually occur at higher frequencies than in C_{68}^{6-}.

Eisler et al. used the thin sphere model to establish two types of vibrations, the so-called monopolar (referred to as "breathing") and quadrupolar ("squashing") modes,[18] which may be used to characterize the carbon cages by means of their Raman spectra. The squashing mode is fivefold degenerated in the case of an ideal sphere and for an I_h point group, such as C_{60}, but it is split by the symmetry reduction in other fullerenes. The magnitude of the splitting represents the deviation of the cage from sphericity. The

Table 2. Vibrational modes of the Sc_3N cluster in $Sc_3N@C_{68}$.

Symmetry	Frequency	I(IR)	Exptl IR	I(RR)[a]	I(off-RR)[a]	Exptl Raman	PED [%][b]	Description[c]
E	86.3	1.47		91.2	68.0	90 (br m)	82 Sc(z), 9 C_{68}, 9 Sc(x,y)	rot. ($R_{x,y}$)
A_2	114.9	6.95					55 Sc(z), 26 Sc(x,y), 17 C_{68}	transl. (55 % T_z) + rot. (R_z)
A_2	154.4	1.52					60 Sc(x,y), 19 Sc(z), 18 C_{68}	rot. (60 % R_z) + transl. (T_z)
E	166.4	3.26		20.8	27.2	174 (s)	75 Sc(x,y), 18 C_{68}, 8 Sc(z)	Sc-N-Sc bend
A_2	213.0	5.56					93 N(z), 5 Sc(z)	N out-of-plane (pyramidal deformation)
E	241.8	1.15		14.2	51.3	249 (w)	55 C_{68}, 40 Sc(x,y), 5 N(x,y)	transl. $T_{x,y}$
E	305.2	0.00		0.3	25.0	*313 (vw)*	89 C_{68}, 11 Sc(x,y)	transl. $T_{x,y}$
E	327.7	0.41		3.1	3.3	336 (w)	91 C_{68}, 8 Sc(x,y)	transl. $T_{x,y}$
E	343.5	0.50		0.0	6.4		78 C_{68}, 20 Sc(x,y)	transl. $T_{x,y}$
A_1	350.9			0.1	3.4	*361 (vw)*	82 C_{68}, 18 Sc(x,y)	sym. Sc–N stretching
A_1	424.3			24.6	98.8	431 (m)	74 C_{68}, 26 Sc(x,y)	sym. Sc–N stretching
A_1	521.2			7.7	72.9	528 (w)	62 C_{68}, 38 Sc(x,y)	sym. Sc–N stretching
E	638.0	59.36	661 (s)	0.6	1.0	*660 (vw)*	67 N(x,y), 26 C_{68}, 6 Sc(x,y)	asym. Sc–N stretching
E	638.9	17.41	661 (s)	0.0	0.1		79 C_{68}, 20 N(x,y)	asym. Sc–N stretching

[a] Computed intensities are given in % with respect to the most intense lines; I(RR) denotes intensities for resonance Raman scattering. [b] PED (potential energy distribution) analysis shows the contribution of the carbon cage (denoted as C_{68}) and Sc_3N atoms to the given vibration; Sc(z), Sc(x,y), etc. denote contributions of Sc displacements along z or (x,y) directions. In the D_3 group, the contributions from x and y displacements are equivalent and thus are given together. [c] rot. = rotation; transl. = translation; sym. = symmetric; asym. = antisymmetric.

shape of the C_{68} cage deviates significantly from a sphere: the cage is flattened along the C_3 axis, and squashing modes in C_{68} are computed to be at 213 (A_1), 224 (E), and 237 cm^{-1} (E). The splitting (24 cm^{-1}) is close to the value reported for C_{70} (33 cm^{-1}) and is smaller than in most other fullerenes studied by Eisler et al.[18] This pattern is preserved in C_{68}^{6-}, although the frequencies are slightly higher (218 (A_1), 225 (E), 246 cm^{-1} (E)) and the splitting is increased to 28 cm^{-1}. The frequencies of squashing modes of $Sc_3N@C_{68}$ are significantly hardened. The calculated frequency of the A_1 mode is 232 cm^{-1}; in the experimental Raman spectrum it is observed at 239 cm^{-1} (w+). A lower-frequency E mode shifts to 239 cm^{-1} (calcd) and, along with another E mode, contributes to the weak Raman line at 249 cm^{-1}. Finally, the second E mode in $Sc_3N@C_{68}$ is mixed with the cluster vibration and therefore cannot be tracked unambiguously. The highest contributions of this mode are found at 242 cm^{-1} (39 %, measured 249 (w)) and 305 cm^{-1} (37 %, measured 313 (vw)). The hardening of the squashing modes in $Sc_3N@C_{68}$ versus C_{68}^{6-} would be difficult to explain without covalent interactions with the encapsulated cluster. On the contrary, as far as such interactions are concerned, it is inevitable that the cage should become stiffer.

The breathing cage mode is nondegenerated, and its frequency was shown to correlate with the inverse square of the fullerene molecular mass, irrespective of the cage shape. This is also true for the breathing mode in the empty noncharged C_{68} (not shown), for which our calculations predict a frequency of 453 cm^{-1} (Raman), which is less than that in C_{60} (calculated 487 cm^{-1}, measured 496 cm^{-1}), but higher than that in C_{70} (calculated 448 cm^{-1}, measured 455 cm^{-1}).[18] Upon sixfold charging of the empty C_{68}, C_{68}^{6-} is expected to give a 10 cm^{-1} softening on the breathing mode. On the other hand, the breathing mode of the cage in $Sc_3N@C_{68}$ is mixed with the symmetric Sc–N stretching vibrations, and the highest contributions of such a breathing mode are found at 424 cm^{-1} (56 %, exptl 431 cm^{-1} (m)) and 521 cm^{-1} (34 %, exptl 528 cm^{-1} (w)).

On the basis of the IR intensity pattern and the characteristic squashing and breathing modes discussed above, it can be concluded that the effect of Sc_3N encapsulation in the cage is more complicated than just a formal transfer of six electrons, and the vibrational spectra of the carbon cage in $Sc_3N@C_{68}$ cannot be adequately understood on the basis of the C_{68}^{6-} cage solely.

Vibrations of the adjacent pentagons: Because of the unique non-IPR carbon cage in D_3-$Sc_3N@C_{68}$,[9] the vibrations of the three pairs of adjacent pentagons (Figure 8a)

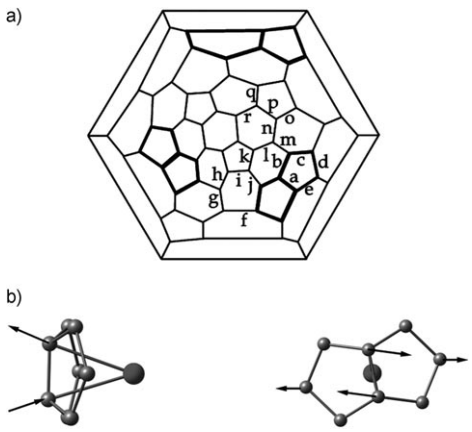

Figure 8. a) Schlegel diagram of C_{68}. The adjacent pentagons are shown in bold. b) Vibrational displacements (only major contributions are shown) for "swinging" mode of "a" bonds (left; 791 (E), 789 cm^{-1} (A_2)) and the A_1 vibration at 792 cm^{-1} (right), which most probably corresponds to the strong Raman line at 806 cm^{-1}.

are quite intriguing. A list of all modes of $Sc_3N@C_{68}$ with contributions from 24 carbon atoms in the adjacent pentagons exceeding 50 % (note that in the case of uniform distribution of the vibration over the whole cage this contribution should be 24/68 = 35 %) is given in Table S3 of the Support-

ing Information. Most of the vibrations with enhanced localization on the pentagons have low intensities. The only exception is the strong Raman line at 806 cm^{-1}, which may be assigned either to E symmetry "swinging" vibration of the "a" bonds with the vibrational displacements illustrated in Figure 8b (left) or to the A_1 mode with 50% contribution from pentagons, which can be roughly described as "rotation" of the "a" bonds around the Sc–N axis (Figure 8b, right). Unfortunately, the calculations do not seem to describe the intensities in this range adequately, and all assignments are rather ambiguous. Taking into account the resonance character of the Raman scattering, intensities of the A_1 modes are expected to be higher owing to the Franck–Condon principle. In the IR spectra, the "swinging" mode of the "a" bonds appears at 800 cm^{-1} (either A_2 or E modes, which are quasidegenerated). This swinging mode is the only vibration localized solely on the adjacent pentagons.

Conclusion

In summary, we have synthesized the non-IPR fullerene $Sc_3N@C_{68}$ in a high yield by using the "reactive gas atmosphere" method. The established facile route enabled us to study the electronic and vibrational structures of $Sc_3N@C_{68}$ by absorption and vibrational spectroscopy for the first time and to compare them with theoretical calculations. Its electronic structure was characterized by using UV/Vis/NIR spectra as well as TD-DFT calculations. The observed absorption bands are assigned to specific electronic transitions. The measured IR and Raman spectra exhibit good agreement with the theoretically calculated spectra. A detailed assignment is given for the vibrational modes, including the Sc_3N cluster modes, cage modes, and vibrations of the adjacent pentagons. This study reveals that the effect of Sc_3N encapsulation in the cage is much more complicated than just a formal transfer of six electrons, and consequently, the electronic and vibrational spectra of the carbon cage in $Sc_3N@C_{68}$ cannot be adequately understood on the basis of a C_{68}^{6-} cage alone.

Experimental Section

General procedures for the synthesis of $Sc_3N@C_{68}$ by means of a modified Krätschmer–Huffman DC-arc discharging method with the addition of NH_3 (20 mbar) have been described elsewhere.[1,2,4–7] After DC-arc discharging, the soot was pre-extracted into acetone and further Soxhlet-extracted into CS_2 for 20 h. Fullerene separation was performed by single-stage HPLC on a Hewlett–Packard instrument (series 1050) with toluene as the eluent. A linear combination of two analytical 4.6×250 mm Buckyprep columns (Nacalai Tesque, Japan) was applied to separate the product. The fullerenes were detected by UV at $\lambda = 320$ nm. The purity of the isolated products was checked by HPLC runs performed on a 10×250 mm Buckyclutcher column (Regis, USA), followed by LD-TOF MS analysis running in both positive-ion and negative-ion modes (Biflex III, Bruker, Germany).

Sample preparation and experimental details for UV/Vis/NIR and FTIR spectroscopic measurements have been previously described.[5–7] The Raman spectra were recorded at 4.2 K on a T64000 triple spectrometer (Jobin Yvon, France) with visible laser radiation (Innova 300 series, Coherent, USA) and an excitation wavelength of 676 nm.

Computational methods: Optimized geometry parameters, force fields, and IR intensities of the $Sc_3N@C_{68}$ molecule and the C_{68}^{6-} anion were calculated at the DFT level of theory with the PRIRODA package[19,20] using the Perdew–Burke–Ernzerhof (PBE) functional[21] and the TZ2P-quality basis set with an SBK[22] effective core potential for Sc atoms. The quantum-chemical code employed expansion of the electron density in an auxiliary basis set to accelerate evaluation of the Coulomb and exchange-correlation terms.[19] Off-resonance Raman intensities were computed numerically at the PBE0[23] level with the 6-31G basis set for carbon atoms and the 6-31G* basis set for the Sc_3N cluster. The PC version[24] of the GAMESS (US) package[25] was used for these computations.

The resonance Raman intensities were computed by means of the method described in refs. [26] and [27]. In brief, if there is no normal mode rotation and frequency change in the excited states, the Raman intensity of the ith vibrational mode from the resonance with the S_j excited state is proportional to the square of the displacement parameter B_{ij}, which is defined by Equation (2):

$$B_{ij} = 0.172\omega_i^{0.5}\Delta X_{0,j}\mathrm{M}^{0.5}\mathrm{L}_i \quad (2)$$

in which ω_i is the frequency of the ith vibrational mode, $\mathbf{\Delta X_{0,j}}$ is the vector defining the change in the Cartesian coordinates between the ground and S_j excited states, **M** is the diagonal matrix of atomic masses, and $\mathbf{L}_i$ is the vibrational eigenvector (in mass–weight Cartesian coordinates). The evaluation of B_{ij} by using Equation (2) requires optimization of the geometry parameters for excited states, which causes severe difficulties for large molecules owing to increased computational demands and root-flipping problems. The simplified approach for computation of B_{ij} used in this work was introduced in ref. [27], and is shown in Equation (3):

$$B_{ij} = 2.41 \times 10^6 \omega_i^{-1.5} E'_j \mathrm{M}^{-0.5}\mathrm{L}_i \quad (3)$$

in which E'_j is the gradient of the excited-state S_j computed for the ground-state geometry. We used a time-dependent (TD) PBE functional with a TZ2P basis set implemented in the PRIRODA package to calculate the excitation energies and gradients of the excited states.

Acknowledgements

We cordially thank Ms. K. Leger, Mr. F. Ziegs, and Mrs. H. Zöller for technical assistance and Dr. M. Krause for valuable discussions. S.Y. and M.K. thank the Alexander von Humboldt (AvH) Foundation for financial support. The support of a Volkswagen Foundation (grant I-77/855) and computer time for A.P. at the Research Computing Center of the Moscow State University are gratefully acknowledged.

[1] L. Dunsch, M. Krause, J. Noack, P. Georgi, *J. Phys. Chem. Solids* **2004**, *65*, 309–315.
[2] For a recent review, see L. Dunsch, S. Yang, *Small*, submitted.
[3] S. Stevenson, G. Rice, T. Glass, K. Harich, F. Cromer, M. R. Jordan, J. Craft, E. Hajdu, R. Bible, M. M. Olmstead, K. Maitra, A. J. Fisher, A. L. Balch, H. C. Dorn, *Nature* **1999**, *401*, 55–57.
[4] L. Dunsch, P. Georgi, M. Krause, C. R. Wang, *Synth. Met.* **2003**, *135*, 761–762.
[5] L. Dunsch, P. Georgi, F. Ziegs, H. Zöller, German Patent DE 10301722 A1, **2003**.
[6] a) S. F. Yang, L. Dunsch, *J. Phys. Chem. B* **2005**, *109*, 12320–12328; b) S. F. Yang, L. Dunsch, *Angew. Chem.* **2006**, *118*, 1321–1324; *Angew. Chem. Int. Ed.* **2006**, *45*, 1299–1302; c) S. F. Yang, L. Dunsch, *Chem. Eur. J.* **2006**, *12*, 413–419.

[7] a) M. Krause, L. Dunsch, *ChemPhysChem* **2004**, *5*, 1445–1449; b) M. Krause, J. Wong, L. Dunsch, *Chem. Eur. J.* **2005**, *11*, 706–711; c) M. Krause, L. Dunsch, *Angew. Chem.* **2005**, *117*, 1581–1584; *Angew. Chem. Int. Ed.* **2005**, *44*, 1557–1560.
[8] C. R. Wang, T. Kai, T. Tomiyama, T. Yoshida, Y. Kobayashi, E. Nishibori, M. Takata, M. Sakata, H. Shinohara, *Nature* **2000**, *408*, 426–427.
[9] S. Stevenson, P. W. Fowler, T. Heine, J. C. Duchamp, G. Rice, T. Glass, K. Harich, E. Hajdu, R. Bible, H. C. Dorn, *Nature* **2000**, *408*, 427–428.
[10] M. M. Olmstead, H. M. Lee, J. C Duchamp, S. Stevenson, D. Marciu, H. C. Dorn, A. L. Balch, *Angew. Chem.* **2003**, *115*, 928–931; *Angew. Chem. Int. Ed.* **2003**, *42*, 900–903.
[11] S. S. Park, D. Liu, F. Hagelberg, *J. Phys. Chem. A* **2005**, *109*, 8865–8873.
[12] J. U. Reveles, T. Heine, A. M. Köster, *J. Phys. Chem. A* **2005**, *109*, 7068–7072.
[13] J. M. Campanera, C. Bo, J. M. Poblet, *Angew. Chem.* **2005**, *117*, 7396–7399; *Angew. Chem. Int. Ed.* **2005**, *44*, 7230–7233.
[14] H. Shinohara, *Rep. Prog. Phys.* **2000**, *63*, 843–892.
[15] *Endofullerenes: A New Family of Carbon Cluster* (Eds.: T. Akasaka, S. Nagase), Kluwer Academic Publishers, Dordrecht, **2002**.
[16] R. Bauernschmitt, R. Ahlrichs, F. H. Heinnrich, M. M. Kappes, *J. Am. Chem. Soc.* **1998**, *120*, 5052–5059.
[17] M. Krause, H. Kuzmany, P. Georgi, L. Dunsch, K. Vietze, G. Seifert, *J. Chem. Phys.* **2001**, *115*, 6596–6605.
[18] a) H.-J. Eisler, S. Gilb, F. H. Heinnrich, M. M. Kappes, *J. Phys. Chem. A* **2000**, *104*, 1762–1768; b) H.-J. Eisler, F. H. Heinnrich, S. Gilb, M. M. Kappes, *J. Phys. Chem. A* **2000**, *104*, 1769–1773.
[19] D. N. Laikov, *Chem. Phys. Lett.* **1997**, *281*, 151–156.
[20] D. N. Laikov, Y. A. Ustynyuk, *Russ. Chem. Bull.* **2005**, *54*, 820–826.
[21] J. P. Perdew, K. Burke, M. Ernzerhof, *Phys. Rev. Lett.* **1996**, *77*, 3865–3868.
[22] W. J. Stevens, M. Krauss, H. Basch, P. G. Jasien, *Can. J. Chem.* **1992**, *70*, 612–630.
[23] C. Adamo, V. Barone, *J. Chem. Phys.* **1999**, *110*, 6158–6170.
[24] A. A. Granovsky, PC GAMESS; URL: http://classic.chem.msu.su/gran/gamess/index.html
[25] M. W. Schmidt, K. K. Baldridge, J. A. Boatz, S. T. Elbert, M. S. Gordon, J. H. Jensen, S. Koseki, N. Matsunaga, K. A. Nguyen, S. J. Su, T. L. Windus, M. Dupuis, J. A. Montgomery, *J. Comput. Chem.* **1993**, *14*, 1347–1363.
[26] Y. Achiba, K. Kikuchi, M. Muccini, G. Orlandi, C. Ruani, C. Taliani, R. Zamboni, F. Zerbetto, *J. Phys. Chem.* **1994**, *98*, 7933–7935.
[27] F. Negri, G. Orlandi, F. Zerbetto, M. Z. Zgierski, *J. Chem. Phys.* **1995**, *103*, 5911–5918.

Received: February 23, 2006
Published online: July 21, 2006

